Mechanical Design of a Self-Mooring Autonomous Underwater Vehicle

Robert C. Briggs

Thesis submitted to the Faculty of the
Virginia Polytechnic Institute and State University
in partial fulfillment of the requirements for the degree of

Master of Science
in
Aerospace Engineering

Wayne L. Neu, Chair
Daniel J. Stilwell
Craig A. Woolsey

December 7, 2010
Blacksburg, Virginia

Keywords: Autonomous Underwater Vehicle, Self Mooring, AUV

Mechanical Design of a Self-Mooring Autonomous Underwater Vehicle

Robert C. Briggs

(ABSTRACT)

The Virginia Tech self-mooring autonomous underwater vehicle (AUV) is capable of mooring itself on the seafloor for extended periods of time. The AUV is intended to travel to a desired mooring location, moor itself on the seafloor, and then release the mooring and return to a desired egress location. The AUV is designed to be an inexpensive sensor platform. The AUV utilizes a false nose that doubles as an anchor. The anchor is neutrally buoyant when attached to the AUV nose. When the vehicle moors it releases the false nose, which floods the anchor making it heavy, sinking both the anchor and AUV to the seafloor. At the end of the mooring time the vehicle releases the anchor line and travels to the recovery location. A prototype vehicle was constructed from a small-scale platform known as the Virginia Tech 475 AUV and used to test the self-mooring concept. The final self-mooring AUV was then constructed to perform the entire long duration mission. The final vehicle was tested successfully for an abbreviated mission profile. This report covers the general design elements of the self-mooring AUV, the detailed design of both the prototype and final AUVs, and the results of successful field trials with both vehicles.

Acknowledgments

I would like to thank the entire Self-Mooring AUV team at Virginia Tech. Developing and designing the new AUV was a collaborative effort and would not have been possible without everyone who was involved. First, Dr. Wayne Neu and Dr. Daniel Stilwell deserve a great deal of thanks for organizing and advising the team. Thanks to Brian McCarter for basically handling all the electronics of the AUV by himself. I would also like to thank Tim Pratt and Chris Bright for their help with the mechanical design. Thanks to Richard Duelley for designing the propulsion system for the final AUV, as well as handling all the seal testing. Jason Mims also deserves a big thanks for his advice on design and his help with the structural analysis. All photos and figures are owned by the Autonomous Systems and Control Laboratory at Virginia Tech.

Contents

List of Figures

List of Tables

List of Symbols

A : cross-section area

b : span

C : length of straight sides on anchor

c : chord

C_d : coefficient of drag

C_f : coefficient of friction

D : depth

d : diameter

e : energy

η : efficiency

FF : form factor

F_d : drag force

ℓ : length

∇ : displaced volume

ν : water viscosity or Poisson's Ratio

P : pressure

p : power

q : external pressure

R : CEP Radius

r : radius

R_e : Reynold's number

ρ : density

SF : safety factor

S_{wet} : wetted surface area

σ : normal stress

T : time

t : thickness

T_{naca} : airfoil thickness fraction

V : volume

v : velocity

W : weight

x : longitudinal position

y : vertical position

List of Abbreviations

AUV : autonomous underwater vehicle

AHRS : attitude heading reference system

CB : center of buoyancy

CEP : circular error probable

CFD : computational fluid dynamics

CG : center of gravity

CPU : central processing unit

FEM : finite element method

GPS : global positioning system

ID : inner diameter

LCB : longitudinal CB location

LCG : longitudinal CG location

LED : light emitting diode

MATLAB : matrix laboratory (software)

NACA : National Advisory Committee for Aeronautics

NPT : national pipe thread

OD : outer diameter

PSU : power supply unit

RF : radio frequency

RPM : rotations per minute

Chapter 1

Introduction

For a number of data collection operations, it is desirable to be able to deploy an autonomous underwater vehicle (AUV) which can travel to a predetermined location, station keep for an extended time and then return to a recovery location. To accomplish this an AUV was developed that is capable of mooring itself on the seafloor. The Virginia Tech self-mooring AUV utilizes a false nose that acts as an anchor. By releasing the false nose the vehicle becomes heavy and sinks to the seafloor. At the end of the data collection mission the mooring is released and the AUV can travel to a recovery location. The mooring system was first tested on a prototype AUV, developed on the existing Virginia Tech 475 vehicle, described in detail below. After the concepts were proven, a full size AUV was developed to perform the mission described below. This paper discusses the design of the mooring system, the construction of the prototype, and the design and development of the full size AUV.

Figure 1.1: VT self-mooring AUV during testing off Panama City Beach, Florida.

1.1 Mission Profile

The intended mission profile is separated into four sections: ingress, descent, mooring and egress. During the ingress phase the AUV will travel to a desired mooring location, periodically surfacing to obtain its location and update its navigation estimates. At the end of this ingress phase, the vehicle must be within a specified circular error probable (CEP) of the target location.

At the end point for the ingress stage the vehicle will update it's position using GPS and release the anchor. A mooring line attached to the anchor pulls the AUV toward the seafloor. The final mooring location is required to be within a rather small specified CEP about the last known location on the surface. The maximum depth for mooring was set to 500 meters. The vehicle will remain in the moored configuration while collecting data. The maximum mooring time depends on the payload power requirements and the transit distance. At the end of the mooring time the AUV will release the mooring line and return to a desired egress location. Figure 1.2 shows the intended mission profile.

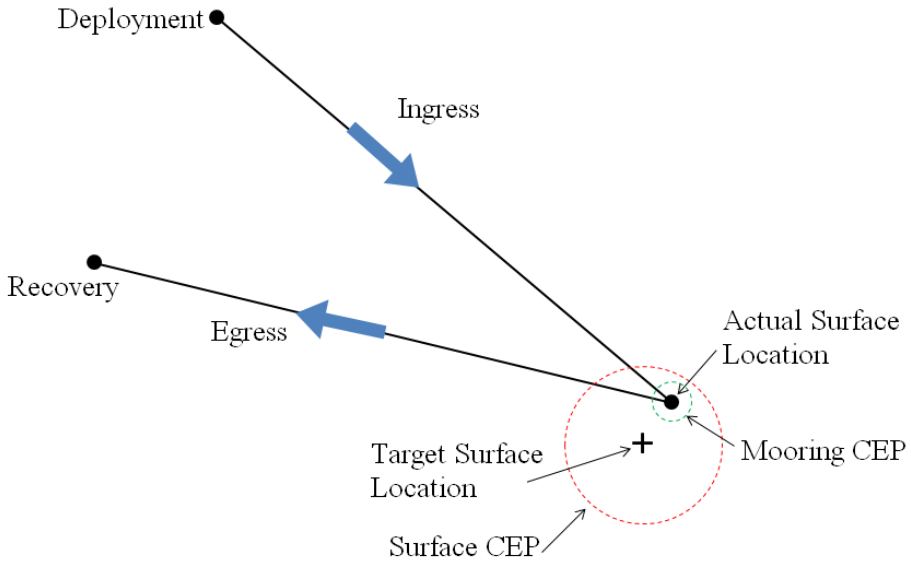

Figure 1.2: Schematic of mooring mission profile. (not to scale).

1.2 Design Approach and Team Structure

In the conceptual design phase the team focused of developing the basics of the anchoring mechanism, including the placement, shape and restraint for the anchor, covered in Chapter 2. To prove the validity of the anchoring mechanism proposed in the conceptual design, a

prototype AUV was developed. The platform used for the prototype was a Virginia Tech 475, shown in Figure 1.3. It is a reliable, small, conventional streamlined AUV which has been previously used for a number of studies. [1, 2, 3] In its base configuration, it is 4.75 inches in diameter, 38 inches long, weighs 18.5 pounds and displaces 18.7 pounds. A motor in the tail drives a single pusher propeller for propulsion. Four individually actuated fin flaps provide control authority. The last stage of the design process was the detailed design and construction of the final self-mooring AUV. This vehicle was based on the prototype, except that it was designed for the full mission.

Figure 1.3: Virginia Tech 475 AUV.

The self-mooring AUV design team was comprised of students and faculty from the Department of Aerospace and Ocean Engineering and the Bradley Department of Electrical and Computer Engineering at Virginia Tech. The acknowledgments at the beginning of this report list all of the team members. Other than the anchor sizing, done by Briggs, all the general design of the AUV was a collaborative effort. The design of the prototype anchor was performed by Briggs and the modifications to the 475 nose were a joint effort between Briggs and Bright. The final AUV mechanical design was mostly performed by Briggs and Pratt. All the electrical design was handled by McCarter, with the exception of the propulsion design, done by Duelley. The structural analysis of the final AUV was performed by Mims and the CFD analysis by Ryan Coe.

Chapter 2

Conceptual Design

The design of the mooring system focused on developing a method that would allow the vehicle to quickly descend, would provide a hydrodynamic and balanced vehicle in all configurations, and be reliable through multiple uses and long mission times. As described in 1.1, the AUV acquires a GPS location at the surface and then releases the anchor. Since currents may push the AUV away from the specified CEP during descent, the anchor must be designed to allow the AUV to descend very quickly. In addition the AUV should be hydrodynamic with and without the anchor. It was decided that the best way to address these issues was to make the anchor a false nose that attaches to the true AUV nose. Adding the anchor in this manner lengthens the vehicle, but does not affect the hydrodynamic shape, allowing for an efficient vehicle with the anchor attached. When the anchor is released it will pull the AUV nose down during descent, minimizing drag and increasing the speed of descent. Figure 2.1 shows the four configurations during the mission.

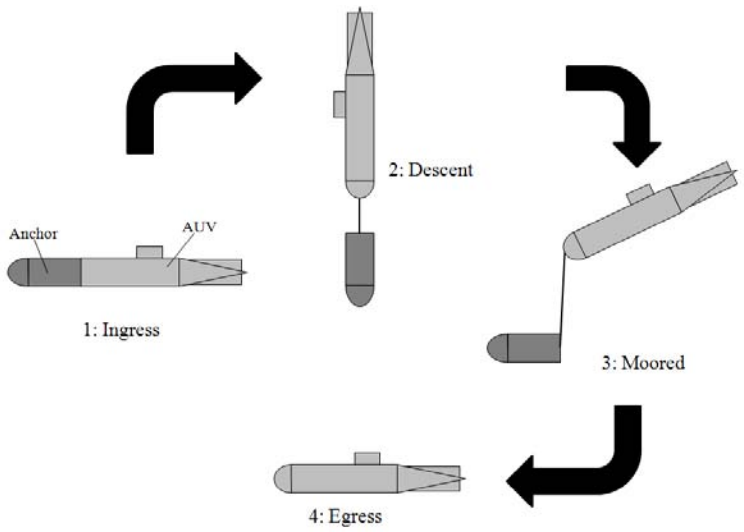

Figure 2.1: Four AUV configurations during proposed mission.

2.1 Anchor Attachment

Two concepts were proposed for attaching the anchor to the nose. One concept was to draw a vacuum inside of the anchor. The pressure differential with the surroundings then forces

the anchor to stay on the nose. This concept is simple and requires very little mechanical hardware. The concern with this method is securing the anchor adequately while still having it separate from the seal easily and fall off when released.

The second concept was a mechanically fastened anchor. The anchor would have a threaded rod that protrudes out the back. This rod is inserted into a hole in the nose and through an external-rotor electric motor. By spinning the motor one way it would pull the anchor onto the nose and seal. Turning the motor the other way would push the anchor off. By sizing the threaded rod correctly it can be assured the anchor will break the seal when released.

Due to the simplicity of the system, the vacuum attached anchor was chosen. Both the prototype and final vehicles were outfitted with this system and it proved reliable.

2.2 Galvanic Release

When the mooring phase of the mission is over the AUV must release the mooring line. This is done with a galvanic release installed on the nose of the AUV. The galvanic release consists of two loops of stainless steel wire, an anode and a cathode. The mooring line is attached to the anode. If a properly polarized voltage difference is applied between the anode and the cathode while the vehicle is in salt water the resulting current will rapidly corrode the anode. [4] After a few minutes the wire will break and the vehicle will be released from the anchor. This method of release proved to be simple and robust.

2.3 Anchor Sizing

Since there is no requirement to moor the AUV in a region of strong bottom currents, the grip of the anchor on the bottom was not a concern. Rather, the anchor size was determined by setting the terminal velocity of the anchor-vehicle system during descent. Figure 2.2 shows the descent profile for a case where the current is split into two separate values. From the surface to a depth of D_1, the current is equal to $v_{cur,1}$. From D_1 to depth D_2, at the seafloor, the current is $v_{cur,2}$. As the vehicle dives the currents will push it away from the surface location, shown by the solid line in Figure 2.2. The vertical velocity of the AUV must be sufficient that it will reach the seafloor in no more time than it takes it to travel laterally a distance equal to the CEP radius, R. This vertical velocity is the required terminal velocity, approximated by Equation 2.1. For anchor sizing the worst case scenario, where the currents are at their maximum values and are acting in the same direction, is considered. For this study the maximum current values were set to $v_{cur,1} = 2$ knots and $v_{cur,2} = 0.5$ knots, transiting at $D_1 = 30$ meters. If the vehicle is assume to reach its terminal velocity

immediately upon beginning its descent, a consideration of travel times yields,

$$v_{terminal} = \frac{v_{cur,1} D_1 + v_{cur,2} \left(D_2 - D_1 \right)}{R} \tag{2.1}$$

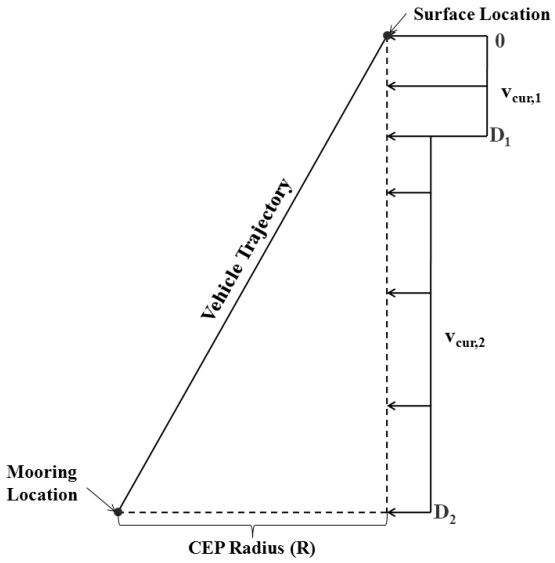

Figure 2.2: Sketch of side drift during descent for a two current case.

Since the submerged weight of the anchor is much greater than that of the submerged egress vehicle it can be assumed that during the descent the two bodies are separated by a few meters (the length of the mooring line), enabling the drag of each body to be treated separately. The anchor is assumed to be shaped like a cylinder with a half sphere front and blunt back, shown in Figure 2.3. This assumption is true for the prototype and was a close enough approximation for the final vehicle. This shape has a coefficient of drag, $C_{d,anchor}$, which is very nearly 0.2 for fineness ratios between 2 and 10. [5] The reference area for this drag coefficient is the cross-sectional area, $A = \pi r^2$. Thus the drag on the anchor is,

$$F_{d,anchor} = \frac{1}{2} \rho v^2 A C_{d,anchor} \tag{2.2}$$

The drag on the AUV ($F_{d,vehicle}$) is separated into two parts: the main body and the sail. The body drag is calculated by the corrected form factor approach. [5] First the coefficient of friction, $C_{f,body}$, is calculated as a function of velocity, v, body length, ℓ, and the kinematic viscosity of water, ν. The friction coefficient used is the 1957 ITTC line. [6]

$$Re_\ell = \frac{v\ell}{\nu} \tag{2.3}$$

$$C_{f,body} = \frac{0.075}{\left(\log_{10} Re_\ell - 2.0 \right)^2} \tag{2.4}$$

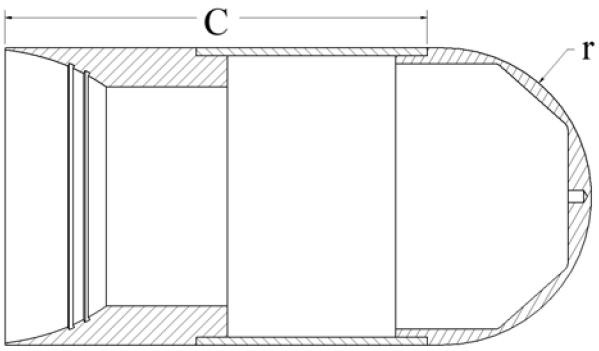

Figure 2.3: Assumed anchor shape.

An appropriate form factor is chosen for the vehicle's shape. Since the prototype will be a modified 475 vehicle and the final vehicle will be based on the 475, the chosen form factor is a cylinder with hemispherical ends. The form factor, FF, is a function of body length, ℓ, and diameter, d.

$$FF = 2.643 + 1.5\left(\frac{d}{\ell}\right)^{1.5} + 7\left(\frac{d}{\ell}\right)^{3} \tag{2.5}$$

The coefficient of drag, $C_{d,body}$, is obtained by multiplying the coefficient of friction, $C_{f,body}$, by the form factor, FF, and, since the reference area for the coefficient of friction is the total wetted surface area, S_{wet}, and for the coefficient of drag is the cross-sectional area, A, the ratio of these areas.

$$C_{d,body} = C_{f,body}\frac{S_{wet}}{A}FF \tag{2.6}$$

Further employing the shape approximation of a cylinder with hemispherical ends, the area ratio is reduced to

$$\frac{S_{wet}}{A} = 4\frac{\ell}{d} \tag{2.7}$$

The drag force on the body is then

$$F_{d,body} = \frac{1}{2}\rho v^2 A C_{d,body} \tag{2.8}$$

The sail drag is calculated by the general airfoil approach. [5] The coefficient of friction, $C_{f,sail}$, is calculated as in Equation 2.4, except the Reynolds number, Re_c, is referenced to the airfoil chord, c.

$$Re_c = \frac{vc}{\nu} \tag{2.9}$$

$$C_{f,sail} = \frac{0.075}{\left(\log_{10} Re_c - 2.0\right)^2} \tag{2.10}$$

The coefficient of drag, $C_{d,sail}$ is obtained by multiplying $C_{f,sail}$ by a ratio of areas which can be approximated as a function of c and airfoil thickness, t. [5] The drag on the sail is calculated as in (2.8) by using $A = cb$, where b is airfoil span.

$$C_{d,sail} = 2\left[1 + 2\frac{t}{c} + 60\left(\frac{t}{c}\right)^4\right] C_{f,sail} \tag{2.11}$$

$$F_{d,sail} = \frac{1}{2}\rho v^2 (cb)\, C_{d,sail} \tag{2.12}$$

The total drag on the vehicle is estimated as the sum of (2.8) and (2.12). The resulting drag is increased by 25% to account for the drag of the fins and transducer. This was empirically determined from previous experiments with the 475 vehicle and is felt to be conservative for both the prototype and final vehicles.

$$F_{d,vehicle} = (F_{d,body} + F_{d,sail}) \times 1.25 \tag{2.13}$$

The total drag of the two body, anchor-vehicle system is just the sum of the anchor and vehicle drags.

$$F_d = F_{d,vehicle} + F_{d,anchor} \tag{2.14}$$

At terminal velocity during descent, the wet weight of the anchor, $W_{a,wet}$, defined as the net weight of the flooded anchor removed from the egress vehicle, must equal the total drag, F_d, of the descending two body system.

$$W_{a,wet} = F_d \tag{2.15}$$

Also, for a properly ballasted ingress vehicle, the dry weight, $W_{a,dry}$, defined as the weight of the unflooded anchor when attached to the egress vehicle or the weight of the ingress vehicle minus the weight of the egress vehicle, must equal the weight of the additional water displaced by the ingress vehicle over that displaced by the egress vehicle. The volume of this additional displacement is equal to the volume of the anchor minus the volume, V_{lost}, occupied by the portion of the egress vehicle's nose that extends into the anchor when it is attached to the egress vehicle. Referring to Figure 2.3, this additional displacement can be written as

$$\nabla_{anchor} = \frac{2}{3}\pi r^3 + C\pi r^2 - V_{lost} \tag{2.16}$$

Thus,

$$W_{a,dry} = \rho \nabla_{anchor} \tag{2.17}$$

Further, for proper trim, the longitudinal center of gravity (LCG) must coincide with the longitudinal center of buoyancy (LCB) for both the egress and ingress vehicles. Assuming the egress vehicle is properly trimmed, the addition of the anchor must shift the LCG and LCB by equal amounts. This means that the LCG of the anchor mass must coincide with the center of volume of the additional displacement, ∇_{anchor}. Further, if the anchor is to fall vertically during descent, its center of gravity must be located on its axis of rotation.

Proper anchor design then requires adjustment of the length, C, and the anchor mass distribution to simultaneously satisfy Equations 2.15 and 2.17 as well as proper placement of the anchor's center of gravity.

2.4 Feasibility Study

After the general design was selected a feasibility study was done to calculate a range of possible dimensions for the final vehicle. This showed what size vehicle would be needed to meet the mission requirements. The first step in the feasibility study was to estimate the batteries needed for a given vehicle size. An egress vehicle would then be found and used to estimate the size of the anchor. Knowing this the properties of the ingress vehicle would be calculated. This process was put into a MATLAB program and iterated until a solution was found for a variety of diameters.

Using an initial vehicle geometry the drag of the vehicle is calculated as described above. The energy needed is then estimated from propulsion, CPU and payload requirements. The propulsion system consumes the most energy, calculated in Equation 2.18, assuming an overall propulsion efficiency of $\eta_p = 40\%$. The energy consumed from the propulsion system is the power required to overcome the drag, $F_{d,vehicle}$, at a specific velocity, v, multiplied by the time the propulsion system is active, T_p. The CPU and sensors are estimated to consume 5 watts while running. To calculate the energy required this power, p_{CPU}, is multiplied by the time the CPU is on, T_{CPU}, which is during the ingress and egress phase (2.19). The energy required by the payload is estimated to be $e_{payload} = 950Wh$, and for this study it was assumed the payload would only be active during the mooring phase. The total energy required is simply the sum of the energy from propulsion (e_p), CPU (e_{CPU}) and payload ($e_{payload}$).

$$e_p = T_p \left(\frac{v F_{d,vehicle}}{\eta_p} \right) \tag{2.18}$$

$$e_{CPU} = p_{CPU} T_{CPU} \tag{2.19}$$

$$e = e_p + e_{CPU} + e_{payload} \tag{2.20}$$

Using this energy requirement and the given battery specs a number of cells can be found and then a size of the battery stack. Knowing an estimate of the size of the batteries, the

CPU, the required sensors and hardware an egress vehicle size and weight is calculated. This information can be used to calculate the anchor size, as above.

Lastly the egress drag, mass and size is calculated. If the calculated vehicle is too heavy, length is added to the vehicle to increase the buoyancy. If the vehicle is too light, mass is added. This process is iterated until a solution is found.

2.4.1 Results

The preceding analysis was run for vehicles with diameters between 4.75" and 7.5". It was assumed the vehicle would travel 50 nm during ingress and egress, at an average velocity of 4 knots. A 0.5 knot head current was assumed during both transit phases.

Table 2.1: Estimated dimensions of self-mooring AUV

Egress Dimensions				Ingress Dimensions			
d**(in)**	ℓ**(ft)**	ℓ/d	**weight (lb)**	d**(in)**	ℓ**(ft)**	ℓ/d	**weight (lb)**
4.75	8.69	22.0	65.04	4.75	10.79	27.3	81.57
5.00	7.55	18.1	61.73	5.00	9.38	22.5	77.82
5.25	6.73	15.4	60.19	5.25	8.37	19.1	75.84
5.50	6.04	13.2	58.64	5.50	7.55	16.5	74.30
5.75	5.48	11.4	57.32	5.75	6.82	14.2	72.97
6.00	5.09	10.2	57.32	6.00	6.36	12.7	73.19
6.25	4.76	9.1	57.54	6.25	5.97	11.5	73.63
6.50	4.49	8.3	57.76	6.50	5.61	10.4	74.30
6.75	4.23	7.5	57.98	6.75	5.31	9.4	74.96
7.00	4.00	6.9	58.42	7.00	5.02	8.6	75.62
7.25	3.94	6.5	60.85	7.25	4.92	8.1	78.93
7.50	3.97	6.4	65.26	7.50	4.92	7.9	84.22

The results of the feasibility study were used to narrow down possible dimensions of the final self-mooring AUV. It was found that diameters between 5.75" and 7.25" were the best for overall weight, with 5.75" providing the lightest vehicle. However diameters between 6.5" and 7.25" were considered due to the fineness ratio ($\frac{\ell}{d}$). A lower fineness ratio should ensure a more controllable AUV. These rough dimensions were used in the initial design of the final AUV.

Chapter 3

Prototype Vehicle

To validate the decisions made during conceptual design a prototype vehicle was constructed (Figure 3.1). The prototype was capable of the full mission described in Section 1.1, except with a shorter range and no deep diving capabilities. An existing 475 vehicle was modified with expanded payload capacity, an external anchor, galvanic release, and the necessary plumbing to deploy the anchor. Once constructed the prototype vehicle was tested in several phases to prove the various concepts and assumptions made in the design of the self-mooring AUV. First the proper ballast of the ingress and egress configurations was checked, then the diving capabilities were proven, and finally a full system test was completed.

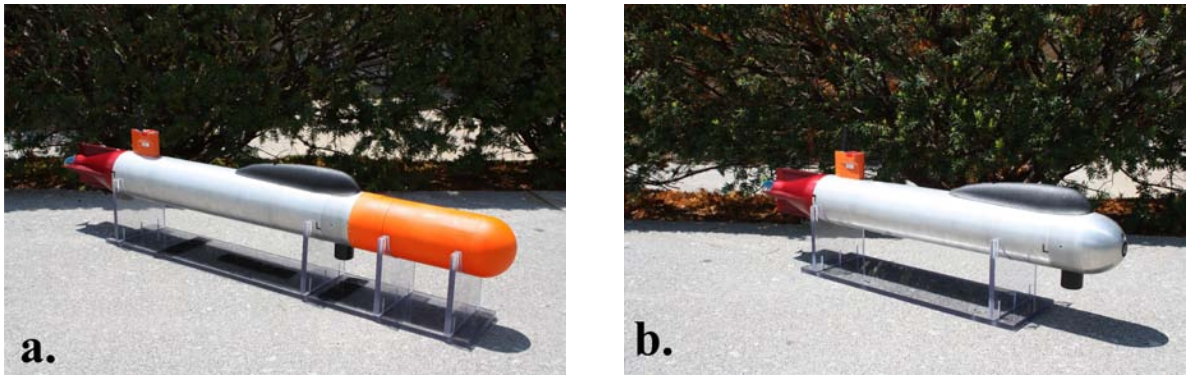

Figure 3.1: Prototype self-mooring AUV in both ingress (a) and egress (b) configurations.

3.1 Payload Integration

To expand the payload capacity for the expected addition of environmental sensors, the tube of the 475 vehicle was extended by six inches for the prototype. The payload was added forward in the vehicle between the new nose and the vehicle electronics chassis. Placing a payload such that the center of gravity of the payload and any required ballast is in line with the center of buoyancy of the six inch extension will keep the AUV balanced.

3.2 Anchor Design

For the prototype vehicle, the descent CEP requirement was set to 75 feet at a depth of 100 feet. This gave the size, weight and desired CG location of the anchor. To achieve the proper CG location while keeping manufacturing as simple as possible, the anchor was split into three parts, a machined front and back, and a polycarbonate tube for the center section. The anchor's front was machined out of steel and the back out of aluminum. The three sections were joined together using silicone sealant. To seal the anchor to the nose of the AUV, the back of the anchor was machined to match the outside contour of the nose. Two o-ring grooves were added to this surface and provided a positive seal.

As a balancing aid, a brass weight ring was added to the anchor. The weight ring was held in the anchor by four thumb screws allowing for easy adjustment fore and aft. For the mooring line that connects the anchor to the galvanic release, Spectra® line was chosen. A small line was needed so winding it inside the anchor would not require much room, and Spectra® offers a great strength to size ratio. The line was wrapped around a plastic cylinder and secured with candle wax. The cylinder was then mounted in the front inside of the anchor. When the anchor is deployed the wax seal breaks and the line unravels until taut. After initial testing it was found that this securing method deploys well, but for stability of the anchor during descent, a three point bridle was added which connects the mooring line well above the CG of the anchor. Figure 3.2 shows the prototype anchor and its design features.

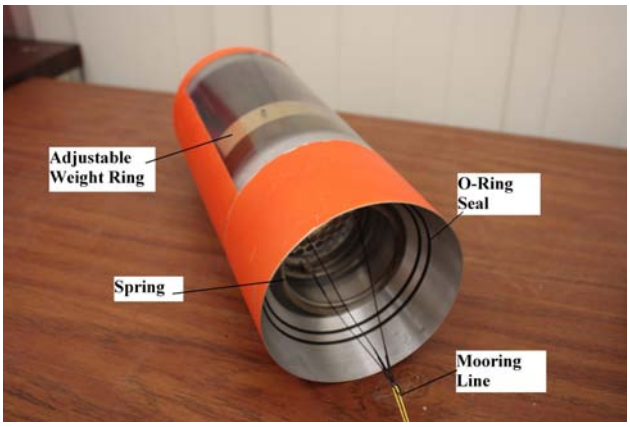

Figure 3.2: Prototype Anchor.

3.3 Nose Modifications

The 475 nose needed to be modified to accommodate both a galvanic release and the vacuum system required for attaching and releasing the anchor. A 1/2" NPT threaded hole was added to the front of the nose to accommodate a galvanic release made from a PVC plug.

The vacuum system relied on an off-the-shelf servo actuated valve used for hobby aircraft. This valve was placed inside the nose and connected to an extra pressure port placed on the front of the nose, above the NPT hole. The other side of the valve was connected to a quick-connect tube fitting placed on the top of the nose. This allowed a vacuum to be pulled in the anchor via the quick-connect fitting. Once a vacuum was established the valve was closed. When releasing the anchor the valve was open, pulling air and/or water in from outside the vehicle and releasing the vacuum.

Early anchor dive testing proved this method was not sufficient. It was found that the valve restricted the flow into the anchor causing the vehicle to sit in place for over a minute waiting for the anchor to fall off. This would allow the vehicle too much time to drift off target. In addition if the anchor pulls in water and becomes heavy the vehicle could start sinking before the anchor was released. This could result in the vehicle gliding horizontally a significant distance before the anchor released. To reduce the anchor release time on the surface, it was decided to increase the diameter of the tubing and valve forming the vacuum system. In addition, a carbon dioxide canister was connected to the exterior vacuum port with flexible tubing. The vacuum release could now be accomplished quickly and without weight change by discharging the compressed CO_2 into the anchor.

To accomplish this modification, a new nose was designed. The new nose exterior was the same as the old nose, however by changing the interior a larger valve could be used. The new valve was a regular 2-way valve modified to be driven by a hobby servo, shown in Figure 3.3. This allowed a much higher flow rate into the anchor. Since the CO_2 canister connected to the outside of the vehicle a fairing was designed to cover it. The fairing can be seen in Figure 3.1

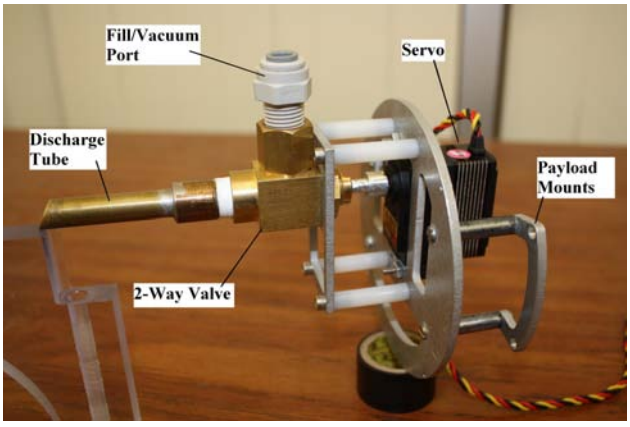

Figure 3.3: Internal components of the prototype vacuum system.

The galvanic release for the new nose, shown in Figure 3.4 was redesigned to be inserted from the front of the nose and seal using an o-ring. This simplified the process of preparing the sub for use and provided a more reliable seal. The galvanic release is modified from an off-the-shelf plastic bolt. For the anode two holes are drilled through the bolt and a loop of

stainless steel wire is inserted. The cathode is a small washer inserted into a groove on the face of the bolt. Wires are attached to the anode and cathode and connected to the vehicle electronics. The galvanic release is sealed to the AUV by an o-ring placed in a groove on the AUV nose.

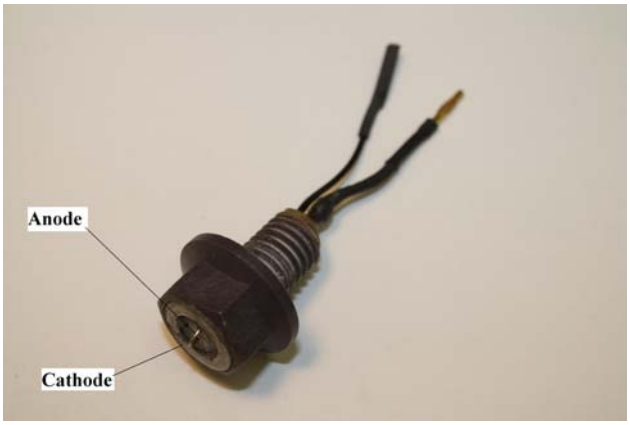

Figure 3.4: Prototype galvanic release.

3.4 Prototype Testing

3.4.1 Dive Testing

The dive testing was done at depths of 30 feet and 60 feet. The testing helped to validate the anchor sizing and release. Experimental measurements of terminal velocity and time to descend are presented in Table 3.1 and Figure 3.5 along with results from simulations of these events used to validate the model developed. The model used for the simulations did not treat the time between the initialization of the anchor release and the mooring line becoming taut. During this time, the egress vehicle loitered near the surface as the mooring line deployed. This process is shown in Figure 3.6. The simulation times were shifted to correspond to the time that the mooring line first pulled the vehicle into its rapid descent during the test. The terminal velocity seen in testing was found to be slightly lower than the simulated terminal velocity however the time to descend was more accurately predicted. The velocity discrepancies may be due to variations in the angle of the AUV during the initial portion of the descent or an underestimate of the total drag of the system.

The small dip at the beginning of the actual descent seen in Figure 3.5 is where the mooring line is unwinding from the anchor. Note the shift in the simulated trajectory to account for this unmodeled phenomenon as discussed above. At the end of the dive the anchor impacts the seafloor, but the AUV continues down. The drag and the buoyancy of the AUV stop it before it reaches the seafloor and then it rises to the mooring height, determined by the

Table 3.1: Simulated vs. Actual Descent Results

	Depth	**Terminal Velocity**		**Time to Descend**	
		Simulated	*Actual*	*Simulated*	*Actual*
Test 1	30 ft.	1.62 m/s	1.25 m/s	10.3 s	9.8 s
Test 2	30 ft.	1.62 m/s	1.2 m/s	11 s	10.8 s
Test 3	60 ft.	1.63 m/s	1.3 m/s	14.8 s	15.6 s

length of the mooring line. The length of the mooring line must be long enough that the vehicle has enough distance to stop, before impacting the seafloor. The AUV fully at rest in the moored configuration is shown in Figure 3.6.

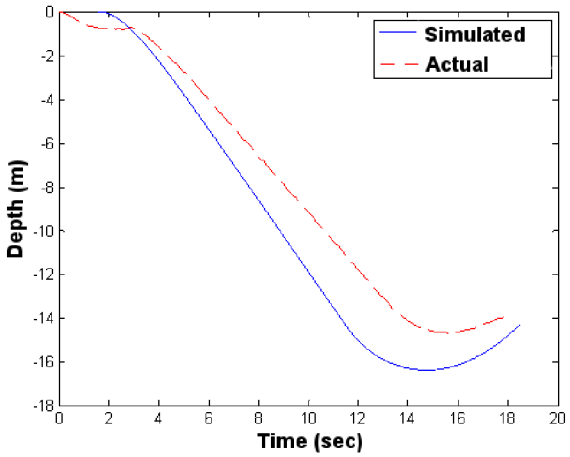

Figure 3.5: Simulated vs. actual descent during the 60 ft. dive test.

3.4.2 Full Systems Test

A full system test was performed twice in the Chesapeake Bay. Both tests were identical. The vehicle was set to have an ingress and egress distance of 1600 meters (1 statute mile). The distance between GPS updates was set to be no more than 350 meters. Figure 3.7 shows the navigation log from the test. The AUV arrived within the CEP at the specified mooring location for both tests. The anchor was then released and the vehicle moored at a depth of 40 feet. After 20 minutes the galvanic release was triggered and the AUV ascended and began the egress phase.

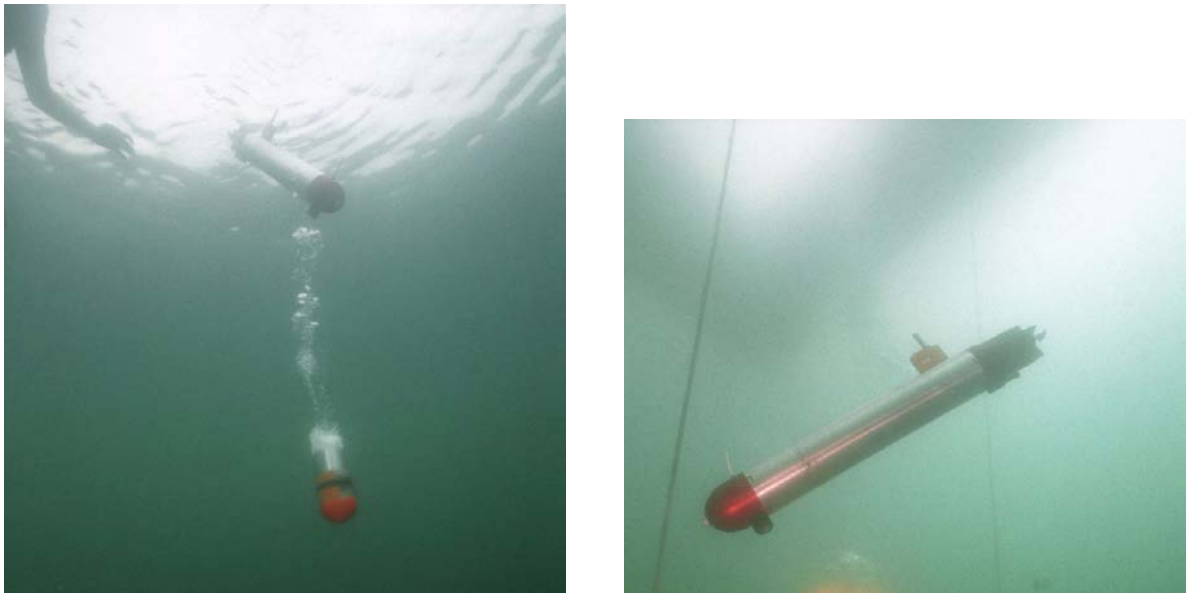

Figure 3.6: Initial deployment of mooring line shortly after anchor release (left) and AUV in the moored configuration (right).

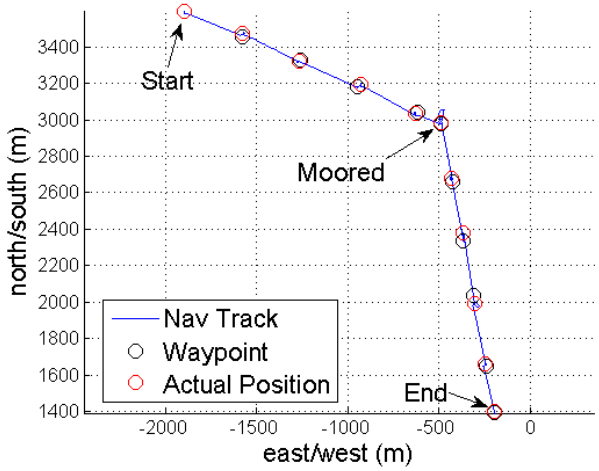

Figure 3.7: Navigation track from full system test.

Chapter 4

Final Vehicle

4.1 Overall Design

After the initial design concepts were proven on the prototype, a full size final vehicle was designed. This vehicle is capable of the full 100 nautical mile mission and is rated to 500 meters depth. The design of the vehicle is based on the prototype vehicle and the 475 vehicle. The final self-mooring AUV is shown in Figure 4.1.

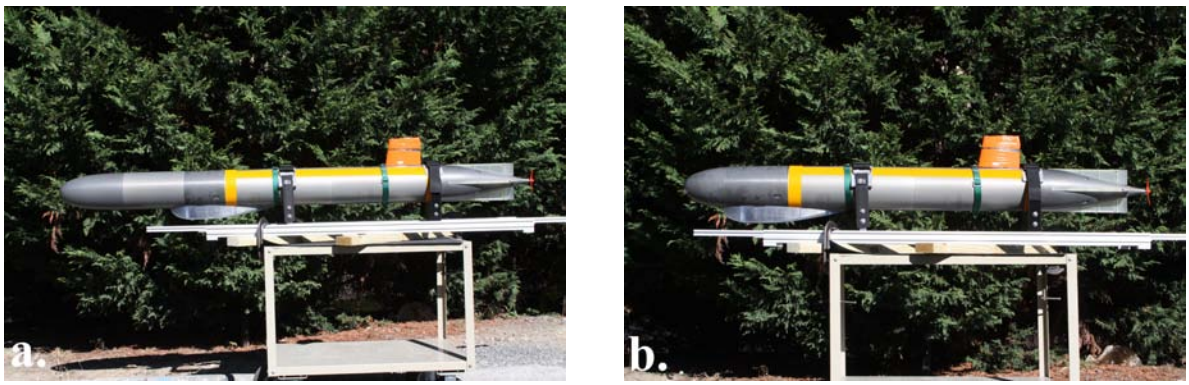

Figure 4.1: Final self-mooring AUV in both ingress (a) and egress (b) configurations.

4.1.1 Configuration

The final self-mooring AUV was designed with the intention to utilize the platform for uses beyond the mooring mission. This meant the design would need to be expandable with the option to add or remove hardware. One way to ensure this was to place all the AUV hardware into the tail. This allows the tail to essentially be a self contained AUV, minus communication antennas and sensors. Thus the tube and nose could be changed for different missions and attached to the same tail. This decision left the nose and tube open for payload and batteries.

4.1.2 Hydrodynamic Design

Placing the AUV electronics in the tail allowed for more flexibility in the outside contour of the vehicle, while still keeping the tube as a parallel mid-body. To simplify the design the DARPA2 submarine geometry, [7] known as the suboff design, was used as a starting point. The normal suboff design is defined by three equations: one for the nose, the parallel mid-body and the tail. Normally the nose and tail length are equal, however to better fit the components the lengths were set independently. [8, 9] Also some constants defining the tail of the sub were varied to fit the electronics better.

The equations describing the suboff geometry are listed below. The lengths r, ℓ, ℓ_{nose}, and ℓ_{tail} are all specified in meters. Since the vehicle is designed in English units these must be converted. The equations for the suboff design vary with x, the distance aft of the nose of the submarine. Calculating the y position, a side profile of the sub was developed. [8, 9] This was revolved around the center axis to give the AUV shape. The suboff shape can be seen in Figure 4.2.

$$\underline{Nose:}$$

$$y(x) = r\left[1 + 0.054x^2(\frac{x}{\ell_{nose}} - 1)^3 - (1 + 0.0393x)(\frac{x}{\ell_{nose}} - 1)^4\right]^{\frac{1}{2.1}} \tag{4.1}$$

$$\underline{Tube:}$$

$$y(x) = r \tag{4.2}$$

$$\underline{Tail:}$$

$$y(x) = r\left[A + B\epsilon^3 + C\epsilon^4 + D\epsilon^5 + E\epsilon^6\right]^{\frac{1}{2}} \tag{4.3}$$

$$where:$$

$$A = r_h^2 + r_h K_0 \epsilon^2$$

$$B = 20 - 20r_h^2 - 4r_h K_0 - \frac{1}{3}K_1$$

$$C = -45 + 45r_h^2 + 6r_h K_0 + K_1$$

$$D = 36 - 36r_h^2 - 4r_h K_0 - K_1$$

$$E = -10 + 10r_h^2 + r_h K_0 + \frac{1}{3}K_1$$

$$r_h = 0.1175$$

$$K_0 = 30$$

$$K_1 = 45$$

$$\epsilon = \frac{\ell - x}{\ell_{tail}}$$

Initially these equations were used directly to develop the outside contour of the nose, tail

and anchor. This method caused problems when being translated to the tools required to machine it. To avoid this the parts were redrawn with multiple constant radius curves that closely matched the equations.

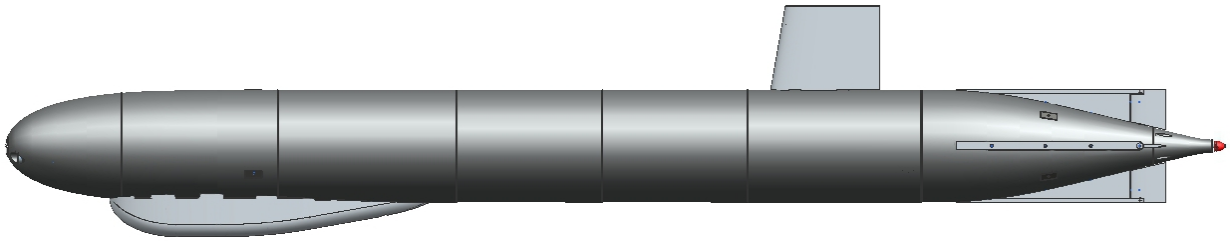

Figure 4.2: Final AUV Shape.

4.1.3 Overall Sizing and Units

It was decided early in the design process to use English units for the AUV. Both metric and English provide difficulties as the rotary seals are only readily available in English and the electronics are mostly specified in metric. However, English was determined as the best solution since most of the raw material and hardware needed are easier to obtain in English dimensions. In addition most machine shops are better equipped to handle English jobs. All the drawings of the AUV are specified in English units and where needed the metric dimensions are converted to English units.

The diameter of the vehicle is set from the battery layout. The battery stack requires an internal diameter of 6.1". A simple wall crush and buckling calculation was done on a tube of this ID, explained in detail in Section 4.4.1. It was found that a tube with an outside diameter of 6.9" was adequate for strength and containing the batteries. This diameter was also chosen so aluminum stock with a nominal OD of 7" could be turned down to give a true concentric OD of 6.9".

The length of the vehicle was estimated early in the design, but left open to changes as the design progressed. The length is mostly a function of how many batteries are needed, so this was left open as drag and added torque from the seal and propeller were calculated. Also as the design progressed it was seen that more flexibility in the longitudinal position of the CB and CG was needed, so the tube was elongated. This allowed the battery weight to be moved slightly forward and aft. As described in Section 4.1.2 the suboff equations were modified to allow the nose and tail length to be set independently. Initially in the design the lengths were set to the default percentages of the total length, as defined for a suboff design. All the electronics were then placed to fit in this area. As the design progressed the tail was shortened to reduce the unused internal volume. In addition the nose was shortened to aid in positioning the CG near the CB.

4.1.4 Tolerances

All dimensions on the vehicle are held to a tolerance of 0.003" unless specified otherwise. Most tolerances on the vehicle are not critical, however all the sealing surfaces are required to be held at a tighter tolerance. These tolerances were specified by the seal manufacturers and added to the part drawings. [10] In addition the bearings for the control surfaces and main shaft required a tighter tolerance.

4.1.5 O-Ring Design

O-Rings are used for all the static seals on the vehicle. O-rings provide a simple and reliable sealing method. In addition they require very little structure and mechanics to implement, keeping the weight of the AUV down. Two styles of o-ring seals are used. The first is the male piston design; where an o-ring is placed in a gland on the male part, which is inserted into the female part. The o-ring seals against the inner diameter of the female part and the outer diameter of the male part. This sealing method is used for all the connections between the body sections, the sail, the galvanic release, and the discharge tube. The second style of seal is a face seal; where an o-ring is sandwiched between a gland on one part and a flat wall on another part. This sealing method is used for the depth sensor and the transducers. [10] The use of a piston seal is favorable over a face seal, since the o-ring stays in place better during installation due to being stretched over the male part.

Piston Seal Sizing

The first step in sizing an o-ring seal is picking the general size of the o-ring. This is usually a factor of the part size and the structure size around the o-ring. Once a general o-ring size is chosen the exact dimensions and tolerances can be found from o-ring sizing guides. To ensure a good seal the o-ring must be compressed by the right percentage, this is done by sizing the o-ring gland and mating parts correctly. Usually an inner diameter of the female part, an outer diameter of the male part, a diameter for the bottom of the gland, and a gland width is specified, shown in Figure 4.3. [10]

In addition to the general sizing, proper precautions against damage to the o-ring must be taken. All the corners on the o-ring glands must be rounded. The top corners are usually just rounded to a radius of 0.005". This just makes them smooth so they don't tear into the o-ring. The bottom corners are rounded to specifications depending on the o-ring cross-section. This not only protects the o-ring, but ensures a good seal. Lastly a chamfer must be added to the inside lip of the female part. This allows the o-ring to be compressed correctly during installation. [10]

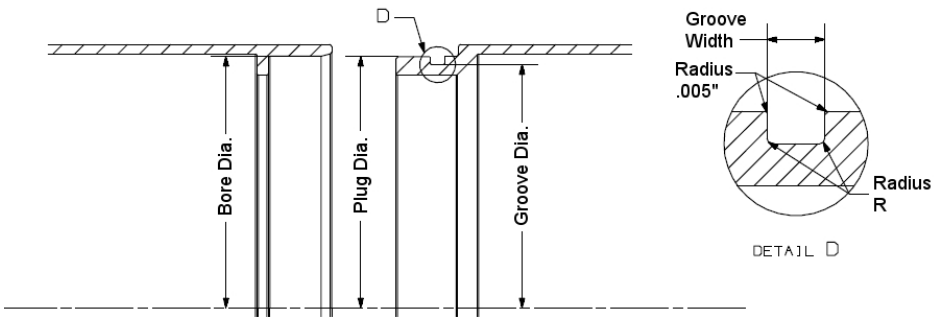

Figure 4.3: Piston Seal Dimensions.

Face Seal Sizing

A face seal is defined in much the same way as the piston seal. The o-ring gland width is determined in the same manner. Also, the corners of the gland are radiused the same. The depth of the gland is determined from the o-ring cross-section.

The diameter of the gland depends on the pressure application, shown in Figure 4.4. If the pressure is pushing the o-ring from the inner diameter, $P1$, the outside diameter of the gland needs to be specified, since it is the sealing surface. The opposite is true for pressure pushing the o-ring from the outer diameter, $P2$. [10] All the face seals in the AUV are dimensioned off the outside diameter of the o-ring.

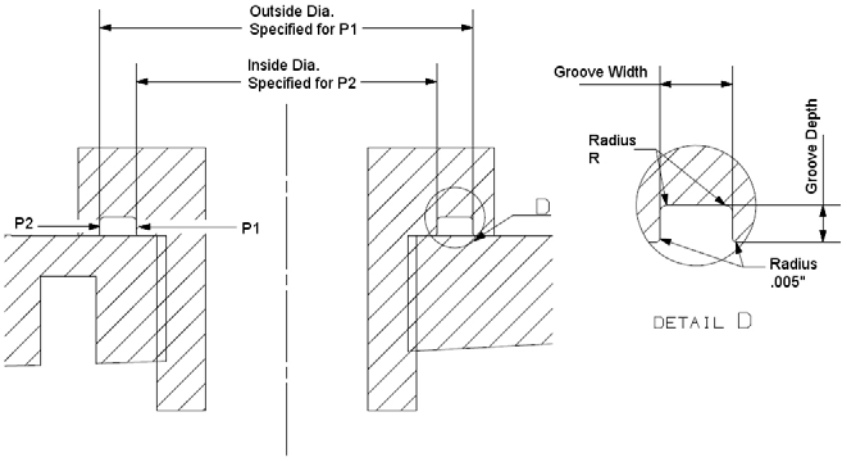

Figure 4.4: Face Seal Dimensions.

4.1.6 Corrosion Resistance

Corrosion on the AUV is caused by an electrochemical reaction between the metal of the AUV hull and the salt water surrounding it. All metal surfaces have imperfections which causes small voltage differences across the material. If this material is submerged in salt water an ion current is produced between the positive region (anode) and negative region (cathode) of the material. If left in the salt water for an extended period of time material will be removed from the anode. As material is removed the properties of the material will change and new anodes and cathodes will be formed. The result will be corrosion across the AUV. [4]

This process of corrosion will occur for a single metal, but if two different metals are in contact the corrosion will occur much more rapidly, due to higher voltage differences. [4] Most components connected to the hull were designed with aluminum or plastic where possible. This proved difficult with the tail strake and fairing screws, as plastic was too ductile and aluminum screws were not available in the correct size. This could be fixed with a slight redesign of screw location. For the depth sensor a plastic isolation plug was used, described in Section 4.3.3.

To address the small imperfections in the aluminum of the AUV hull, all exposed metal was anodized with a type 3 hard coat. This provides excellent scratch resistance and isolates the aluminum from the salt water. The default material color for type 3 anodizing is a dark gray. Due to time constraints colored anodizing was not considered. All tolerances apply after anodizing, and since the anodizing process adds material, the parts need to be machined smaller than specified. During manufacturing it was found that maintaining the tolerances in holes on the vehicle was difficult. To address this all the toleranced holes on the vehicle (discharge tube, galvanic release, sail, control surface seals, and main shaft seals) were left bare metal. A method of maintaining tolerances in these locations will need to be found to avoid all corrosion issues.

The last preventative measure for corrosion is cathodic protection. Seven small zinc plates (three on the nose and four on the tail) are attached to the nose and tail of the vehicle with stainless steel screws. The zinc plates purposely create a voltage difference and act as the anodes. [4] This way during the mission the sacrificial plates will corrode before the AUV hull. To ensure electrical connection between the hull and the anode a small external tooth washer is placed between them. To reduce the drag they are all recessed into pockets on the hull.

4.2 Tail Design

The overall tail design is based on the 475 vehicle. The main tail is made of two pieces: a machined cone like structure that houses the electronics and a small tail cone that hold

the seals and bearings for the main motor shaft. The tail cone is essential because it allows access the the flap-servo connections. For stability and control there are four static fins and four movable fins placed around the tail at 90 degree increments. As described above the tail houses all the essential AUV hardware other than the communication antennas and sensors. This includes the CPU, the power supply, the inertial sensor, all the communication modems, and the motor and servos.

4.2.1 Fin Design

Both the static fins and movable flaps are designed to fit within the 6.9 inch diameter vehicle and are manufactured from cast plastic. This reduces the weight of the components and for large production quantities, will reduce the cost. The static fins are attached to the tail by three screws that thread into blind holes on the tail. These screws were originally intended to be plastic, however they proved to be too weak and were replaced with stainless steel.

Making the flaps out of plastic enabled them to have a complicated cross-section. The flaps are NACA 0009 airfoils with the trailing edge removed to ease manufacturing. [11] Equation 4.4 defines the NACA profile of the flap, where c is the chord and T_{naca} is the thickness fraction or the NACA number divided by 100. [12] The flaps are designed to slide over an 1/8" shaft and attach via a set screw. This allows the servos on the inside of the tail to drive the control surfaces. A small spring seal is used to seal where the shaft penetrates the hull. A bearing below the seal and a bearing placed in the static fin hold the shaft in place.

$$y(x) = \frac{T_{naca}}{0.2} c \left[0.2969 \sqrt{\frac{x}{c}} - 0.126 \left(\frac{x}{c}\right) - 0.3516 \left(\frac{x}{c}\right)^2 + 0.2843 \left(\frac{x}{c}\right)^3 - 0.1015 \left(\frac{x}{c}\right)^4 \right] \quad (4.4)$$

The first iteration of the movable flap called for a straight bottom edge, leaving a gap between the hull and flap. CFD analysis, shown in Figure 4.5 was performed on the flaps and showed that a significant portion of the flow was being routed through this gap when the control surface was actuated. By removing this gap the control surfaces could be more effective, resulting in smaller deflections and less induced drag. The bottom of the flaps was redrawn to follow the contour of the tail.

4.2.2 Propulsion System

The propulsion system for the final AUV was designed to use one of two motors from Neu-Motors. The system is designed to work with either the 1521-10.5Y or 1925-3Y. The 1925 motor provides slightly better efficiency (4%) and less weight. Both motors will be tested to decide on a final configuration. [13] The motors were ordered with a custom motor shaft to extend the shaft past the servo basket. The motor shaft is not held to the tolerances

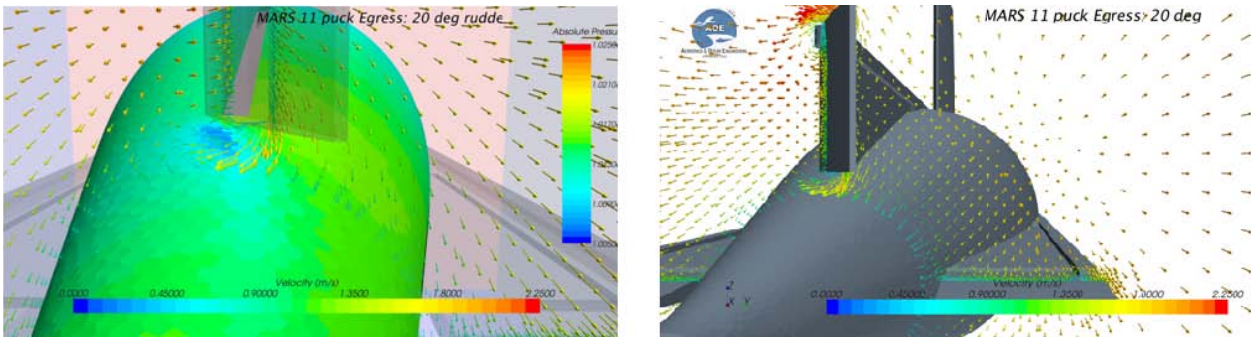

Figure 4.5: CFD analysis of rudder fins before modification. (Used with Permission, Ryan Coe, personal communication, April 1, 2010)

needed by the main shaft seal, so a second custom made stainless shaft is coupled to the motor shaft. This shaft passes through the main shaft seal and bearing. The propeller for the AUV, shown in Figure 4.6 is a custom fabricated propeller specifically designed for the intended mission and propulsion setup. The propeller is designed with a semi-circular hole in the hub, which fits over a matching flat on the end of the main shaft and is then secured with a screw.

Figure 4.6: Final AUV Propeller.

The main shaft is sealed with a spring shaft seal placed in the end of the tail cone. The spring seal is required to seal against 750 psi of pressure, while keeping the added torque to a minimum. Several seals were tested, including custom and off-the-shelf parts, using a small pressure vessel and torque gauge. It was found that a custom seal from Bal Seal provided the best seal and adequately low torque. [13] To accommodate the seal a counterbore is placed on the aft end of the tail cone. The main shaft bearing is an off-the-shelf ball bearing and is inserted into a counterbore placed on the forward end of the tail cone. Both the main shaft seal and bearing are covered by small plates to retain the seal/bearing and keep contaminants out.

4.2.3 Electronics and Motor Chassis

The tail contains all the AUV specific electronics in two chassis. The motor chassis is situated in the aft section of the tail and contains the motor, the speed controller, RPM counter and servos. The AUV electronics chassis is forward of the motor chassis and holds the power supply unit (PSU), central processing unit (CPU), the communication modems and the attitude heading reference system (AHRS). The two chassis are designed to connect with a custom interconnect board. This allows the chassis to be removed easily for repairs and eliminates the requirement for long wires. The front bulkhead of the electronics chassis doubles as the locking mechanism for the tail-tube connection. Three tabs on this bulkhead match the breakaway bulkhead (Section 4.4.3) in the tube.

4.3 Nose Design

Originally the nose was designed as a single piece, however this proved too hard to manufacture and heavy. The nose was then split into two parts that would be welded after construction. Finite element analysis showed the weld joint was barely strong enough for the pressures expected so it was decided to replace it with an o-ring seal. This proved very effective and only added a small amount of weight over the welded option. The nose houses the Benthos transducer (for external communications), shore power connector and depth sensor. These all protrude from the bottom of the nose and are covered with a hydrodynamic fairing.

4.3.1 Air System Design

The air system is similar to the one developed for the prototype. Since the vehicle will be traveling at depths of 500 meters, it will be subjected to near freezing temperatures. If the vehicle is filled with regular air the moisture will condense and possibly damage the electronics. To avoid this the AUV will be filled with dry nitrogen gas. Since the nitrogen will be available it is used to release the anchor as well.

The port used to pull the vacuum has been removed from the nose and placed on the anchor itself (see Section 4.5). This was done due to the long nose and the complexity of routing a port far back on the nose. The two-way valve of the prototype was replaced with a three-way valve. This allows a vacuum to be pulled on the AUV. It also gives the option of scuttling the AUV by opening this port and flooding the vehicle.

4.3.2 Galvanic Release

The final galvanic release works the same way as the prototype. One of the main problems with the prototype galvanic release was wires breaking while screwing the release into the nose. This was fixed in the final by making the galvanic release a simple plug with an o-ring. The plug is custom designed and cast out of plastic. In this system the plug gets inserted without twisting and then screwed into place. Two interconnect boards were designed to connect the galvanic release to the nose chassis, shown in Figure 4.7. This simplified the installation process. The release was also redesigned with two loops of stainless steel wire, instead of one loop and a washer. This made building the release in house easier and faster. The galvanic release also acts as a vacuum release valve for the vehicle. By removing the galvanic release a vacuum inside the vehicle can be released without needed electrical power to the vehicle. The final galvanic release is shown in Figure 4.7.

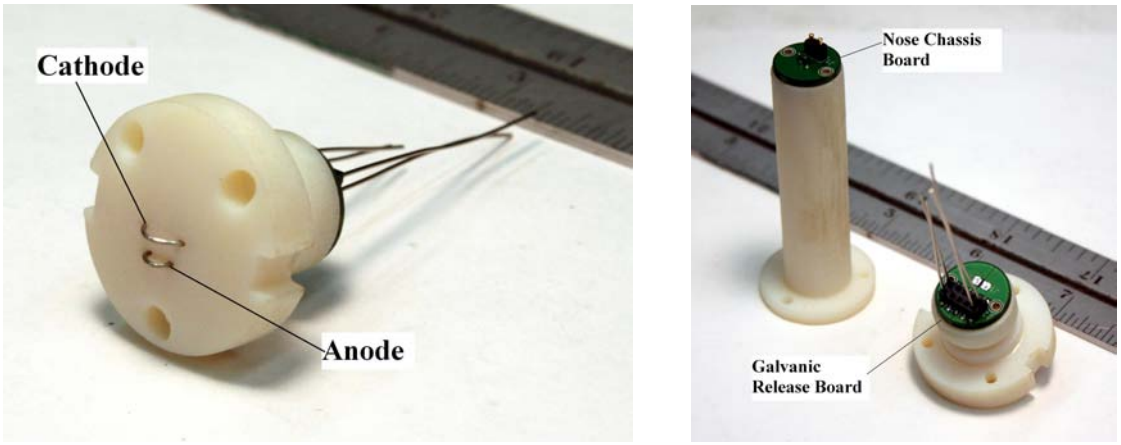

Figure 4.7: Final galvanic release (left) and detail of interconnect system (right).

4.3.3 External Antennas and Connections

The transducers, the shore power connector and the depth sensor were all mounted in the nose, due to its thick wall and available space. The Benthos transducer is off-the-shelf and mounted accordingly. The shore power connector chosen was a Seacon XSEE-BCR, with 12 number 20 connections. This was the smallest Seacon connector with the required connections. The depth sensor chosen was a stainless steel pressure sensor. To avoid the stainless steel sensor from contacting the aluminum hull a small plastic isolation plug was constructed. This plug screws into the hull from the inside and seals with an o-ring. The depth sensor then screws into the plug and seals against it.

A fairing (Figure 4.8) was designed to cover all the equipment protruding from the hull. It was sized to cover the Benthos transducer and avoid separation of flow. The fairing mounts to both the nose and tube, so it must be installed after the vehicle is assembled.

Figure 4.8: Final AUV Fairing

4.4 Tube Design

The tube of the AUV is with internal ribs to strengthen the body while adding a minimal amount of weight. This design requires machining on the inside diameter of the tube, which makes a single piece tube very difficult to construct. The original design was made with a four part tube joined by welding after manufacturing. Finite element analysis showed this would not be strong enough for the pressures expected, so the design was changed to o-ring joints. This strengthened the tube and only increased the weight slightly. Each joint between the tube sections was replaced with a single o-ring and four bolts to hold them together. Since the joints between the tube and nose/tail are taken apart frequently, they were made double o-ring seals. This just adds extra security against wear on one of the o-rings. The two middle sections of tube were designed to be identical to simplify manufacturing.

4.4.1 Rib Spacing and Sizing

Early in the design process the outer and inner diameter of the tube were set to 6.9" and 6.1", respectively. This provided room for the battery packs on the inside and allowed the outside of the sub to be machined out of 7" stock. To design the structure of the tube a stress analysis was done while varying the rib spacing and width. This analysis was done by Jason Mims. The first part of the analysis was calculating the yield stress for failure by crushing. This was done by calculating the normal stress, σ_T, on the thin-wall tube. This stress is calculated from the three-component stress on the tube, using the Von Mises yield equation (4.8). Figure 4.9 shows the unit convention for the three stresses, σ_1, σ_2, and σ_3. [14] The equations below calculate the stress at the given external pressure, q, of 750 psi. Since σ_2 is a maximum at $r = r_{inner}$ and σ_3 is a maximum at $r = r_{outer}$, the location of the total maximum stress is not known. [14] Thus the calculation was run at ten values of r between r_{inner} and r_{outer}. Using the tensile yield stress, σ_{yield}, of aluminum (6061 of 3.99×10^4 psi),

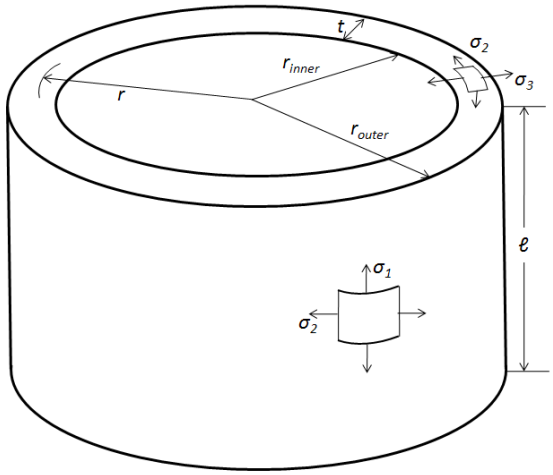

Figure 4.9: Dimensions and stress conventions of tube stress analysis.

the safety factor of the tube can be found.

$$\sigma_1 = \frac{-qr_{outer}^2}{r_{outer}^2 - r_{inner}^2} \tag{4.5}$$

$$\sigma_2 = \frac{-qr_{outer}^2(r_{inner}^2 + r^2)}{r^2(r_{outer}^2 - r_{inner}^2)} \tag{4.6}$$

$$\sigma_3 = \frac{-qr_{outer}^2(r^2 - r_{inner}^2)}{r^2(r_{outer}^2 - r_{inner}^2)} \tag{4.7}$$

$$\sigma_T^2 = (\sigma_1^2 + \sigma_2^2 + \sigma_3^2) - \sigma_1\sigma_2 - \sigma_2\sigma_3 - \sigma_1\sigma_3 \tag{4.8}$$

$$SF_{crush} = \frac{\sigma_{yield}}{\sigma_T} \tag{4.9}$$

The second part of the analysis is finding the external pressure at which elastic buckling occurs, q', calculated in Equation 4.10. [14] To calculate q' the Young's modulus, E, and the Poisson's ratio, ν, of the material is needed. Equation 4.10 also requires the number of lobes formed by the tube during buckling. The normal way to account for this is the calculate q' for $2 \leq n \leq 10$, and use the minimum value of q'. From experimental results the recommended critical pressure, P_{crit}, occurs at 80 percent of the minimum q' value. [14] The safety factor for failure by buckling is calculated using P_{crit} and the expected external pressure, q.

$$q' = \frac{E\frac{\ell}{r_{outer}}}{1+\frac{1}{2}\left(\frac{\pi r_{outer}}{n\ell}\right)^2}\left[\frac{1}{n^2\left[1+\left(\frac{n\ell}{\pi r_{outer}}\right)^2\right]^2}+\frac{n^2t^2}{12r_{outer}^2(1-\nu^2)}\left[1+\left(\frac{\pi r_{outer}}{n\ell}\right)^2\right]^2\right] \quad (4.10)$$

$$P_{crit} = 0.80q' \quad (4.11)$$

$$SF_{buckling} = \frac{P_{crit}}{q} \quad (4.12)$$

To find the rib spacing and width the stress analysis was first performed on a tube with no ribs. The wall thickness was adjusted to keep both safety factors, SF_{crush} and $SF_{buckling}$ above 2. This gave the wall thickness needed if no ribs were used. Then a number of ribs were chosen, which gave the rib spacing (knowing the tube length). Ignoring the rib width, which is unknown, the rib spacing was used as ℓ in the stress analysis. This gave the wall thickness of the sections between the ribs.

The rib width is then determined by equating the bending stiffness of the tube with ribs to the tube without ribs. Since both tubes are made of the same material this means equating the moment of inertias. This produced a tube with a 0.125" thick wall and seven 0.25" thick, 0.5" wide ribs.

4.4.2 Sail Design

The sail is designed to house all the communication antennas and hold them out of the water while the AUV is on the surface. Also the sail houses the LEDs used as a strobe for locating the AUV. The sail must keep all the antennas completely water tight and provide a seal between the sail and tube of the vehicle. In addition the material of the sail must be transparent to both the radio frequencies of the antennas and visible light. The height of the sail was set to 1.5 times the radius of the vehicle to ensure the antennas will be out of the water. The cross-section of the sail is a NACA 0018 and is defined by the Equation 4.4. [11, 12]

The first design of the sail was a plastic shell with slots for each antenna and the LEDs. The antennas simply dropped in from the bottom of the sail and it was potted using a two component epoxy from Epic Resins (R3526/H5094-01). The sail would then be attached to the vehicle with screws and a gasket. This design proved to be impractical for several reasons. The first was the mounting to a tube. The use of a gasket did not provide a reliable seal. Also this mounting method did not provide much rigidity if the sail was struck by something. Another problem with the sail design was the potting. Large air bubbles formed above the antennas weaking the structure and degrading the antennas' performance. The

first sail potted showed deformation due to the heat produced by the epoxy. The epoxy used for the potting compound has a cure time of 30-40 minutes, which makes the epoxy temperature rise significantly.

The second design fixed the mounting issue by replacing the gasket with a custom bolt. This bolt held the sail to the tube mechanically while providing a seal with an o-ring. This proved to be a much more durable and reliable seal. The middle rib on the back tube section was lengthened to accommodate the o-ring seat for the bolt. The sail was thickened all around to prevent deforming and decrease the effect air bubbles would have on the structural integrity. Lastly the antennas were mounted to an internal structure that slid into the sail. This made installing the antennas easier and allowed the potting compound to be poured before inserting the antennas. Pouring the potting compound in first prevents air from being trapped above the antennas.

In addition the potting compound was changed to Ultraclear 438. This epoxy had a longer curing time (overnight), which reduced the heat produced during curing. An ice bath during curing was used with the old Epic Resins epoxy, which helped reduce air bubbles, but the new potting compound proved sufficient without the need for an ice bath. The potting of the sail was performed in a vacuum chamber to degas the epoxy. This pulls the air out of the epoxy, reducing the number of air bubbles. To facilitate this the shell of the sail was designed to allow paths around the antennas for the air bubbles.

After assembling the sail and testing in the lab it was seen that the sail material degraded signal strength on the GPS and RF antennas enough to hinder field testing. To fix this the sail was modified to have the GPS, Iridium and RF antennas pierce through the top of the sail. The modified sail, shown in Figure 4.10, proved adequate in the field.

Figure 4.10: Final version of the sail

4.4.3 Breakaway Bulkheads

One concern in the final vehicle is a battery fire which would pressurize the inside of the vehicle. To avoid an explosion the breakaway bulkheads, shown in Figure 4.11 that connect the nose and tail to the tube have been designed to fail at a low pressure (<100 psi). Both the nose and tail have three metal tabs which slide into slots on the breakaway bulkheads. The breakaway bulkhead is made of a glass filled urethane that will break easily.

In testing it was seen that the urethane breakaway bulkheads will succumb to creep overtime and break without being pressurized. This concern is partially eliminated by pulling a vacuum on the vehicle whenever it is assembled. Even with this precaution the nose breakaway bulkhead is still stressed when the anchor is attached. To make this connection more secure the nose breakaway bulkhead was replaced with a metal one. This did not sacrifice the protection of the breakaway system since the tail bulkhead remained urethane.

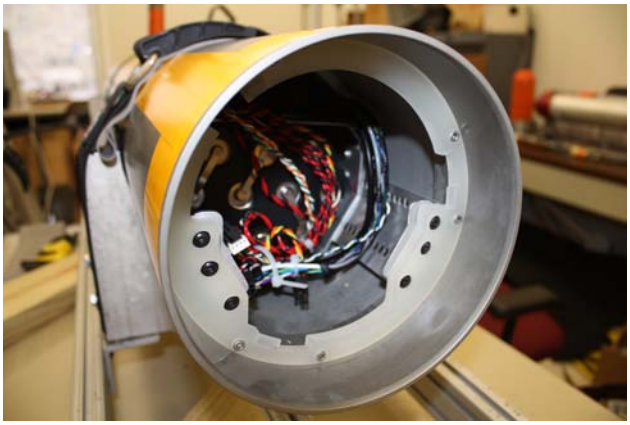

Figure 4.11: Final AUV Breakaway Bulkhead.

4.5 Anchor Design

4.5.1 Shape and Layout

The anchor was designed to have a curved nose section and then parallel sides running back to where is contacts the AUV nose. The curvature of the anchor nose was set to match the AUV nose. On the bottom of the anchor a small cutout was made to accommodate the fairing. The anchor is split into two sections to help with balance and simplify the manufacturing. The two parts are joined together with an o-ring seal. A bulkhead is also attached at the joint between the parts and provides a mooring attachment point. Figure 4.12 shows the anchor in detail.

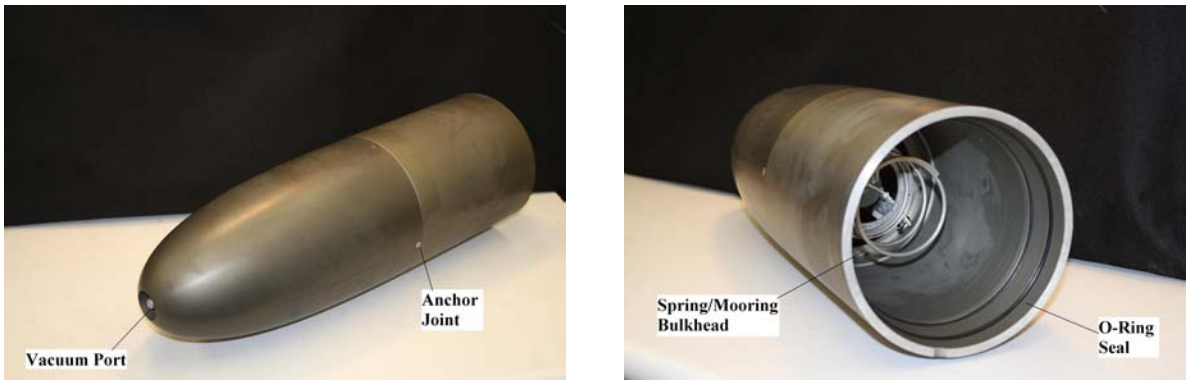

Figure 4.12: Final Anchor.

4.5.2 Weight and Balance

The required weight of the anchor was found using the same method as in the prototype design. The anchor is required to displace the same weight of water as the required weight. Since the anchor shape was set, the length of the parallel section was changed to achieve the correct displacement. The center of buoyancy of this volume is the required center of gravity location.

The internal structure of the anchor is mostly determined by the need to seal against the AUV nose and the joint between the two anchor parts. Through trial and error the thicknesses of all the walls of the anchor were set to match the correct weight and CG of the anchor. The anchor was designed to be slightly buoyant so ballast weight could be added if the balance was off. The anchor structure and estimated CG location is shown in Figure 4.13.

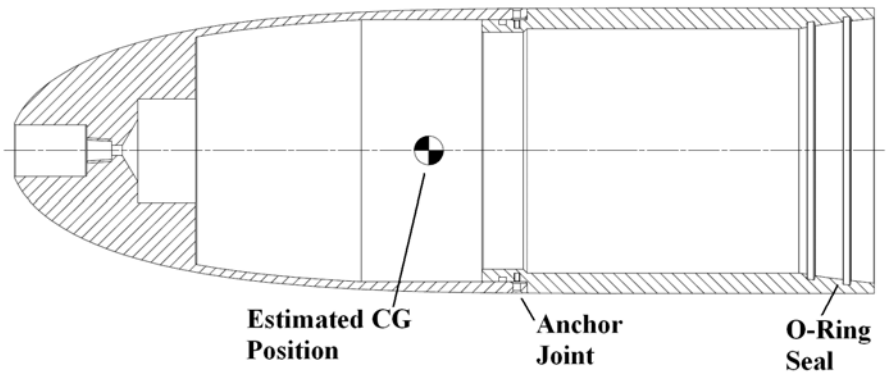

Figure 4.13: Final anchor structure.

When the anchor was machined it was found to be heavier than anticipated. This is most likely due to differences in material properties and the anodizing of the aluminum. To account for this a counterbore was added in the front inside of the anchor to remove weight.

Since the CG-CB separation cannot change, weight was removed by machining down the back lip of the anchor.

4.5.3 Mooring System

The mooring system for the final anchor is based on the lessons learned from the prototype. The mooring line is 500 lb. test Spectra® line, which provides the best strength to size ratio. Three equal lengths of Spectra® line attach the main mooring line to the mooring bulkhead, which is placed in the middle of the anchor above the intended CG location. The line is then wrapped around a cylinder on the mooring bulkhead and secured with wax or tape. To reduce the shock load on the vehicle during anchor release a 12" length of elastic is added to the mooring line at the connection point to the vehicle. The mooring system is shown in Figure 4.14.

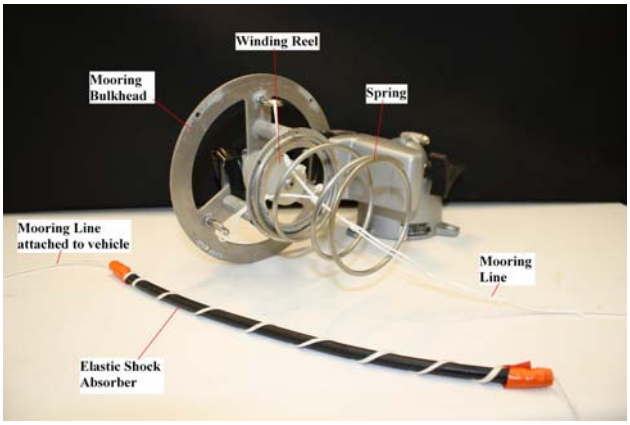

Figure 4.14: Mooring system for final anchor.

4.5.4 Vacuum System

As described in 4.3 the vacuum port has been moved to the front of the anchor. The port selected is a quick connect fitting with an internal valve. This allows the valve to shut off when the vacuum hose is removed. This is essential to avoid any extra plumbing needed in the anchor. The port is located at the front of the anchor to keep it balanced during descent. To reduce drag a small custom cap is installed over the port while not in use. This port also permits the anchor to be released manually by inserting a hose onto the quick connect and releasing the vacuum, an option that was not available on the prototype.

After testing it was seen that the anchor did not release reliably, but would get stuck on the nose of the AUV. This prevented the anchor from flooding and the vehicle would not

descend. To fix this a spring was added to the anchor and attached to the mooring bulkhead. The spring was sized to be compressed when the anchor was attached to the AUV.

Chapter 5

Testing

5.1 Control Testing

The controller on the self-mooring AUV was adapted from the controller developed for the 475 vehicle. [2, 3] Testing was done on the final AUV at Claytor Lake in Virginia to verify the controller's ability to maneuver the AUV. It was seen that the controllability of the vehicle while in transit was extremely good, and the vehicle had significant control authority. The vehicle followed the commanded pitch, depth and yaw very closely. This showed that a new controller would not be needed for the self-mooring AUV. Dive performance was adequate, but will need further work. The yaw control is not active during dive. This can be seen in the 14 degree turn in Figure 5.1. This can be corrected by enabling the yaw controller during the diving portion of the mission. After diving under the surface the AUV overshoots the commanded depth by 1 meter. This overshoot is the same for all depths commanded and can be reduced by tuning the outer depth control loop. The pitch of the vehicle is commanded at 15 degrees nose down during diving. The vehicle drives on the surface for approximately 20 seconds before submerging and quickly pitching down to 15 degrees. At this point the controller determines the vehicle has submerged and reduces the pitch command to the the cruise pitch of 0 degrees.

5.2 Full Mission Testing

The final self-mooring AUV was tested off Panama City Beach, Florida. Due to logistical concerns the testing was done with shorter legs than planned and at a shallower depth. All the dive testing was performed at 60 feet. This also allowed divers to retrieve the anchor.

A full mission was not performed, but an ingress phase to a mooring location was demonstrated. The anchor was released and the vehicle successfully dove to 60 feet. After remaining moored for two hours the galvanic release was triggered. After two minutes the galvanic release burned through and the AUV surfaced. No egress mission was performed.

The mooring system worked as expected, however the anchor release was more explosive than seen in tank testing. While not mission critical the cause of this is unknown. The vehicle dove to the mooring depth quickly, traveling at 1.7 m/s. The pitch angle during mooring was seen to be 34 degrees. Figure 5.2 and Figure 5.3 show the pitch and depth during the descent and ascent, respectively.

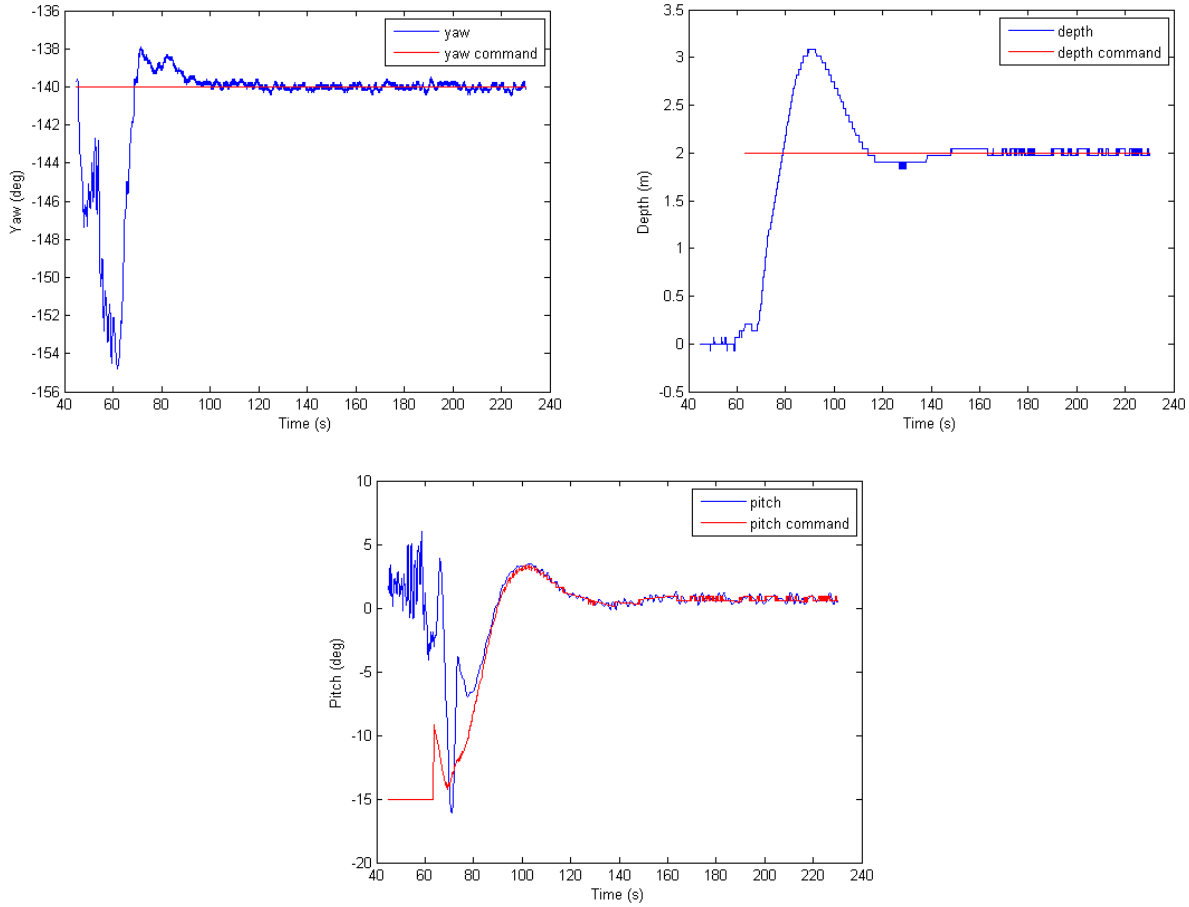

Figure 5.1: Commanded and measured yaw (left), depth (right) and pitch (bottom) during testing.

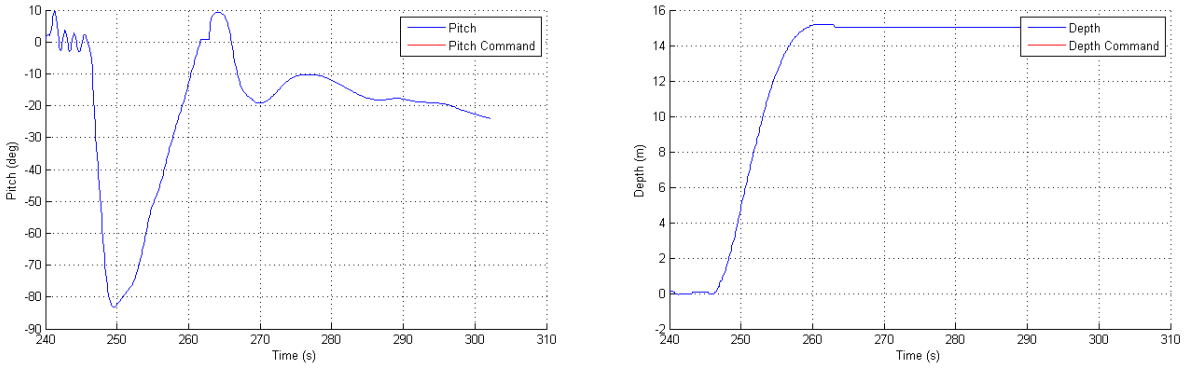

Figure 5.2: Pitch (left) and depth (right) during descent.

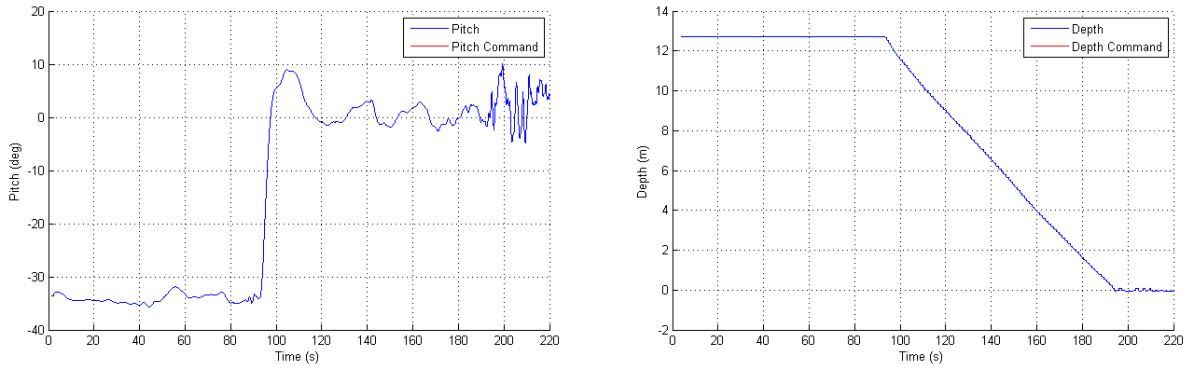

Figure 5.3: Pitch (left) and depth (right) during ascent.

Bibliography

[1] Gadre, A.S., D.K. Maczka, D. Spinello, B.R. McCarter, D.J. Stilwell, W.L. Neu, M.J. Roan, J.B. Hennage. Cooperative localization of an acoustic source using towed hydrophone arrays, in *Proc. IEEE Workshop on Autonomous Underwater Vehicles*, Woods Hole, MA, 2008.

[2] Petrich, J., W.L. Neu, and D.J. Stilwell. Identification of a simplified AUV pitch axis model for control design: Theory and experiments. In *OCEANS 2007, Proceedings of MTS/IEEE*, Vancover, BC, Canada, 2007.

[3] Petrich, J., and D.J. Stilwell. Model simplification for AUV pitch-axis control design, in *Journal of Ocean Engineering*, 37(7): 638652, 2010.

[4] Sackinger, William, *Causes and Prevention of Marine Corrosion*, Marine Advisory Bulletin No. 10, University of Alaska, Fairbanks, Alaska, 1980.

[5] Hoerner, S.F., *Fluid-Dynamic Drag*, Hoerner Fluid Dynamics, Bakersfield, CA, 1992.

[6] ITTC (1957), Proc. 8th ITTC, Madrid, Spain, published by Canal de Experiencias Hidrodinamicas, El Pardo, Madrid.

[7] Groves, N.C., T. Huang, M. Chang. *Geometric Characteristics of DARPA Suboff Models*, David Taylor Research Center, Bethesda, MD, 1989.

[8] Granlund, K., *Steady and Unsteady Maneuvering Forces and Moments on Slender Bodies*, Doctoral dissertation, Virginia Polytechnic Institute and State University, Blacksburg, Virginia, 2009.

[9] Whitfield, C., *Steady and Unsteady Force and Moment Data on a DARPA2 Submarine*, Masters thesis, Virginia Polytechnic Institute and State University, Blacksburg, Virginia, 1999.

[10] "Parker O-Ring Handbook.", Parker Hannifin Corporation, Cleveland, OH, 2007.

[11] Jacobs, E.N., K.E. Ward, R.M. Pinkerton. *The characteristics of 78 related airfoil sections from tests in the variable-density wind tunnel*, National Advisory Committee for Aeronautics Report No. 460, 1935.

[12] Moran, J., *An Introduction to Theoretical and Computational Aerodynamics*, Dover Publications, Inc., Mineola, NY, 2003.

[13] Duelley, R., *Autonomous Underwater Vehicle Propulsion Design*, Masters thesis, Virginia Polytechnic Institute and State University, Blacksburg, Virginia, 2010.

[14] Young, W.C., *Roark's Formulas for Stress & Strain*, McGraw-Hill, Inc., New York, NY, 1989.